Robust Superamphiphobic Coatings with Gradient and Hierarchical Architecture and Excellent Anti-flashover Performances

Yi Xie[1,*], Wei Xiong[1], Shefiu Kareem[1], Chuxiong Qiu[1], Yongfei Hu[1], Ivan P. Parkin[2], Shengwu Wang[3], Huayun Wang[4], Junwu Chen[3], Lee Li[3], Zhi Chen[5], Huajun Sun[1], and Xiujian Zhao[1]

[1] State Key Laboratory of Silicate Materials for Architectures, Wuhan University of Technology, No. 122, Luoshi Road, Wuhan 430070, P. R. China.

[2] Department of Chemistry, University College London, London WC1H 0AJ, U.K.

[3] State Key Laboratory of Advanced Electromagnetic Engineering and Technology (Huazhong University of Science & Technology), No.1037, Luoyu Road, Wuhan, P. R. China.

[4] State Grid Jiangxi Electric Power, Company, Ltd., Electric Power Research Institute, P. R. China.

[5] Wuhan Shuneng New Material Co., LTD, Wuhan, P. R. China.

*Address correspondence to Yi Xie, xiey@whut.edu.cn

Graphical Table of Contents

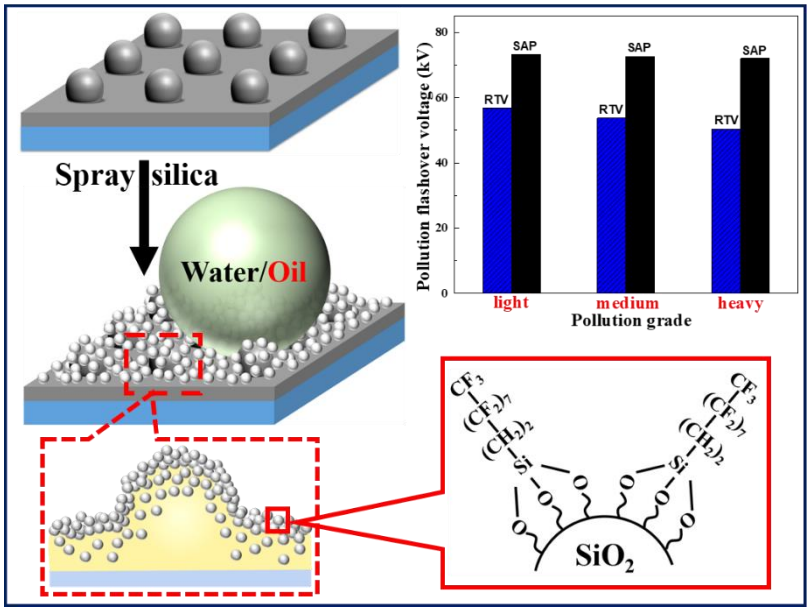

An anti-flashover material was developed by fabricating a robust superamphiphobic coating with unique gradient and micro-nanoscale hierarchical textures.

ABSTRACT

Biomimetic superhydrophobic (SH) coatings have emerged as a promising alternative to traditional room temperature vulcanizing (RTV) silicone rubber coatings for improving the flashover strength of insulators. However, organic contamination occurs in outdoor applications and thus a superamphiphobic (SAP) surface is more desirable but not yet reported for improving flashover performance. Herein, we developed a novel anti-flashover technique by fabricating robust SAP coating with unique gradient and micro-nanoscale hierarchical architecture. The SAP coating was fabricated by sequentially spray-depositing a resin-based primer and a silica-based topcoat on substrates (i.e., glass slides and insulators). The primer not only functions as an adhesive offering strong adhesion to the substrate but also offers a micromastoid-like structure facilitating the subsequent formation of hierarchical micro-nanostructure. The appropriate spraying pressure leads to a diffusion of the fluorocarbon-modified silica nanoparticles into the primer to form a unique gradient structure, by analogy to inserting bullets into a wood. These features render the SAP coating excellent robustness with strong abrasive resistance, excellent UV resistance, chemical and extreme thermal stability. Pollution flashover property of the SAP coating was explored and compared with that of SH and RTV specimens, from which a novel organic-contamination model to evaluate the flashover performance was proposed. The coated SAP glass insulator demonstrated 42.9% pollution flashover voltage improvement than RTV-coated insulator. These stated unique features reveal the convincing potential of the present SAP coatings to be applied for not only outdoor transmission line insulators for anti-flashover but also other fields for self-cleaning, anti-fouling and anti-icing.

KEYWORDS

Superamphiphobic coatings, superhydrophobic coatings, insulator, pollution flashover voltage, anti-flashover

1 Introduction

Fabricating room temperature vulcanizing (RTV) silicone rubber coatings (denoted as RTV hereafter) on hydrophilic surface of glass or porcelain insulators has been investigated to decrease the risk of unplanned line outages [1]. Water repellency of the RTV surface inhibits the formation of continuous and conductive water films and consequently decreases the chance of flashover in electrical power transmission systems [2]. However, RTV coatings have some serious drawbacks such as poor mechanical strength and erosion performance; RTV coatings might gradually degrade and peel off from the original insulator and lose their hydrophobic properties [3]; partial physical or chemical damage of the RTV leads to a reduction in the pollution flashover performance [4]. Furthermore, the formation of individual water droplets on RTV surfaces can cause electric field enhancement at the gas-liquid-solid boundary [5], corona discharges and decrease of hydrophobicity. Once the hydrophobicity fades, the insulation material reduces its ability to suppress leakage currents and partial discharges [6].

On the other side, biomimetic superhydrophobic (SH) and superoleophobic surfaces have become an exciting research frontier in academic areas and showed broad perspective in anti-reflection and self-cleaning for photovoltaics [7], liquid separation [8], blood repellent dressing [9], corrosion resistance [10], microwave absorption [11], water-proofing [12], anti-fogging [13, 14], sensor [15], antibacterial [16], stabilizing water-sensitive semiconductor nanocrystals [17], and so on. Particularly, superhydrophobic (SH) coatings were recently developed to be a promising alternative to traditional RTV for enhancing flashover performances [18-23]. Both the numerical simulation and experimental observation have revealed that the SH surfaces had a better effect of electric field shielding compared with that on ordinary surface [18]. It was also verified that SH surfaces fabricated with polydimethylsiloxane (PDMS) could allow the retention of the dielectric strength of insulators under wet conditions [24]. Coating the

insulators with SH materials effectively prevented water adhering on the device surface thanks to the super water-repellent capability, endowing the insulator surfaces with great leakage distance, suppressing the propagation of leakage currents and reducing the possibility of flashover [21, 25]. The direct current (DC) flashover tests confirmed that SH surfaces were effective in inhibiting surface flashover with the sliding of droplets [23, 26]. It is noteworthy that the contamination of electrical devices in outdoor applications involves a wide range of contaminants including organics such as compost and defecation [27, 28]. For example, the adhesion of bird droppings in ambient environments on the surfaces of insulators leads to the accumulation of soluble salts and water, which weakens the pollution flashover performance. Therefore, superamphiphobic (SAP) surfaces, being both SH and superoleophobic, are much more desirable and promising than the surfaces with only water repellency in practical application especially outdoor environment. However, to the best of our knowledge, SAP coatings have not been investigated yet for practical anti-flashover applications due to the poor mechanical strength and durability.

The fabrication of SAP coatings generally involves the roughening surfaces and modification by low surface-free-energy species; usually from fluorinated compounds [29]. With this regard, various approaches such as chemical etching [30], self-assembly [31], templating [32], chemical vapor deposition [33], and spay-coating [32, 34] have been developed to fabricate SAP coatings. Among these protocols, the wet-chemical processes by dip-coating and spray-coating are of particular interest due to the great convenience for large-scale manufacturing with low reliance on equipment [32, 35-37]. Based on the advantages of spraying technique, strategies by analogy to a “paint + spray adhesive” procedure [38-40] have been explored to reinforce the coating adhesion to substrate and enhance the mechanical robustness and durability of the surfaces against abrasion and impact [41].

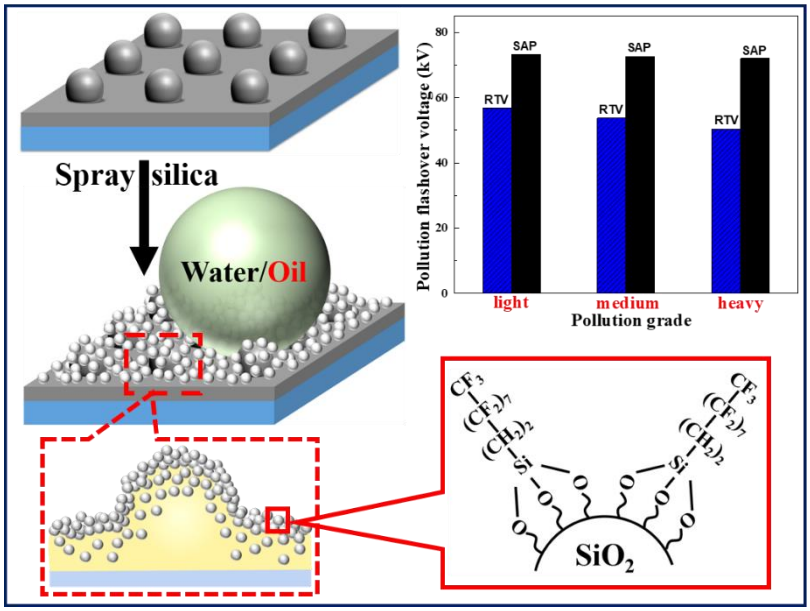

Scheme 1 The schematic diagram for fabricating superamphophobic (SAP) coating with gradient and hierarchical micro-nanostructure, and enhanced pollution flashover strength in comparison with room temperature vulcanizing (RTV) silicone rubber coating.

Motivated by the above-mentioned challenges and inspired by existing research, we developed a novel anti-flashover technique by fabricating a robust SAP coating with unique gradient and micro-nanoscale hierarchical architecture (Scheme 1). The coating was obtained by sequentially spray-coating a resin-based primer and a silica-based topcoat on substrates (i.e., glass slides and insulators), and between the two layers a gradient structure was formed due to the interdiffusion of silica NPs to the primer (Scheme 1). Silica NPs were synthesized by a NaOH-catalyzed procedure and then the NPs surface was modified by low-surface-energy groups in the presence of 1H,1H,2H,2H-perfluorodecyltrimethoxysilane (PFDTMS) (Scheme S1, and Scheme S2a). The primer not only functions as an adhesive to enhance the adhesion but also provides mastoid-like microstructure to facilitate the formation of hierarchical

architecture (Scheme S2b). The self-cleaning properties, thermal stability, UV irradiation stability, chemical stability, mechanical durability as well as the pollution flashover performances of the coated SAP specimens were systematically studied and compared with those of SH and RTV-coated samples. Our work provides a facile and scalable protocol for fabricating SAP coating with not only excellent stability and mechanical durability but also excellent pollution flashover performance, which is promising in practical applications in not only outdoor insulators but also other electrical settings.

2 Experimental

2.1 Materials

Hexamethyl disilazane (HMDS, AR), ethyl acetate (GR，99.5%), butyl acetate (AR) and NaOH (96.0%) were purchased from Aladdin, ethanol (EtOH, AR), tetraethyl orthosilicate (TEOS, AR) from Sinopharm Chemical Reagent Co. Ltd. Hydroxy acrylic resin (HAR) and 1H,1H,2H,2H-perfluorodecyltrimethoxysilane ($C_{13}H_{12}O_3F_{18}Si$, PFDTMS) was purchased from Macklin. Silane coupling agent (KH550) from Suixin Chemical Co. Ltd., Guangzhou. Nylon powder (500 #) was purchased from DuPont. Alkyd resin and polypropylene were purchased from Yoshida Chemical Co. Ltd., Shenzhen. Tetrafluoro resin (HLR-6) was purchase from East Fluorochemical Technology Co., Ltd, Shanghai. All chemicals were used as received without any further purification.

2.2 Preparation of resin-based dispersion

The resin-based dispersion was prepared by mixing several resins in butyl acetate. Typically, alkyd resin (3.0 g) was dissolved in butyl acetate (15 mL) under stirring, followed by sequentially adding polypropylene (0.9 g), tetrafluoro resin (0.5 g) and KH550 solution (0.3 mL, pre-dissolved 0.12 mL KH550 in 0.18 ml H_2O). In order to construct rough micro-surface, nylon powder (1.0 g) was introduced

in the above dispersion and kept the stirring for 12 h to obtain the resin-based dispersion, which will be used for depositing primer. Herein, polypropylene and tetrafluoro resin were introduced to enhance mechanical durability and the adhesion between the whole coating and the substrate. KH550 was introduced to enhance the compatibility between resins and particle fillers (e.g., nylon particle) by crosslinking reaction and thus improve the mechanical durability.

2.3 Synthesis of silica nanoparticle dispersion and nanoparticle surface modification

The silica nanoparticle (NP) dispersion was synthesized at room temperature (RT) by using a modified previously-reported protocol [7]. Typically, a homogeneous solution was prepared by adding 4 mL NaOH (1.8 M, distilled H_2O as solvent) and 100 mL EtOH under stirring. TEOS (20 mL) was then slowly added into the NaOH solution and kept the reaction for 12 h, followed by aging for additional 120 h to obtain a silica NP dispersion. In parallel, a fluorocarbon-based precursor was prepared by dissolving 5 mL of PFDTMS in 100 mL of ethanol. The fluorocarbon-based precursor solution (7.5 mL) was then added in the above silica dispersion and kept stirring for 30 min, followed by adding 20 mL of acid solution (e.g., H_2SO_4 solution with concentration of 0.65 M, HCl or HNO_3 solutions with concentration of 1.3 M) under stirring, which realized the surface chemistry modification of silica NPs with long chain fluorocarbon molecules of PFDTMS. The as-achieved fluorocarbon-modified silica dispersion was used for the subsequent deposition of the topcoat. In order to get different oleophobic degree surface to investigate the influence of oleophobicity on leakage current, different amounts of hydroxyl acrylic resin was also introduced in the silica-based dispersion to fabricate coatings. For comparison, methyl-modified silica NP dispersion was also prepared by using the similar procedure, and HMDS instead of PFDTMS was introduced for the NP surface modification (see details in the SI).

2.4 Fabrication of superamphiphobic and superhydrophobic coatings

Fabrication of SAP and SH coatings was performed under ambient environment (20-30^{o}C, relative humidity ~50-60 %) by sequentially spaying the resin-based primer and the silica-based dispersion on the substrates. The substrates used in this work were pre-cleaned glass slides (7.5 × 2.5 cm or 10.0 × 10.0 cm) and glass insulators (XP-70 with average diameter of 25.5 cm). The silica NPs were pre-modified with methyl groups (for SH coating) or fluorocarbon groups (for SAP coating). Typically, the resin-based or silica-based suspension was spray deposited on vertically positioned substrates using an airbrush with a nozzle diameter of 1.0 mm at a pressure of 2.0-2.5 bar (nozzle to substrate surface distance 15-20 cm). Two and three cycles of spray coating were performed for primer and topcoat, respectively. The resin-based primer layer was kept for evaporation at RT for 2 min before spraying the silica-based topcoat. After spraying, the coatings were dried at RT for 24 h for subsequent characterization and test.

2.5 Materials characterization

The surface morphologies of the various coatings were investigated using a field emission scanning electron microscopy (FESEM, Hitachi S-4800) by keeping the scan rate of 256 Hz. Fourier transform infrared (FTIR) spectra of the representative coatings were analyzed by FTIR (Nicolet 6700, USA) from 4000 to 400 cm^{-1}. Transmission electron microscopy (TEM) images of the as-synthesized silica NPs were acquired on a JEM 2100F (JEOL, Japan) microscope equipped with a field emission gun working at 200 kV accelerating voltage. The samples were prepared by drop-casting NC solutions on 300 mesh Cu grids covered with ultrathin amorphous carbon film. X-ray diffraction (XRD) pattern of the as-synthesized silica NPs was acquired on a Bruker D8 Advanced X-ray diffractometer equipped with a 1.8 kW CuKα ceramic X-ray tube, operating at 40 kV and 40 mA. The static water contact angle (WCA), oil contact angle (OCA), water roll-off angle (WRA) and oil sliding angle (OSA) were recorded on an optical contact angle meter (Theta Lite, Biolin Scientific) by sessile drop method at RT. The WRA and OSA were

measured by tilting the surface until the liquid droplet started to roll off or slide from the surface. Three tests were performed on each coating sample. The volume of droplets for the WCA/OCA and WRA/OSA were 5 μL and 10 μL, respectively.

The UV resistance of the coatings was performed by illuminating the coated glass slides with a UV mercury lamp (UVA-340 lamps, 40 W). The distance between the UV lamp and coating surface was 20 cm. The CAs and SAs were measured every 24 h and the whole illuminating time was 240 h. Chemical stability of the coatings was investigated by immersing the coated glass slides in acidic or alkaline solutions for 168 h. The specimens were rinsed with distilled water and dried at RT, and then the surface wettability was tested. The variation of pH values was tuned from 1 to 14 using H_2SO_4 and NaOH solutions. Regarding the self-cleaning test, the hydrophilic fly-ash particles (45 μm) were used as artificial contaminants. Typically, the coating surface was stained by casting fly-ash particles, followed by dropping water on the surface to investigate the self-cleaning performance.

2.6 Flashover test

The pollution flashover tests of the uncoated glass slide, coated SAP and SH glass slides, and RTV-coated glass slide with sizes of 10 × 10 cm are performed in an artificial pollution flashover platform with a parallel electrode configuration under a rising DC voltage with a ramp rate of 2 kV min^{-1}. Before applied the voltage, the specimens were contaminated by diatomite particles and then fully exposed to saturated moisture in a fog chamber for 15 min by a humidifier. The distance between the two electrodes was 8 cm, and the tilt angle of all coatings was fixed to 15^o during the tests. Every specimen was placed in the same position under the same environment to keep same circumstance for the test. The pollution flashover tests of the various coated SAP and SH glass insulators, and RTV-coated glass insulator followed similar procedures except that AC voltage was applied and gradually raised until flashover occured. The output

voltage, flashover voltage, and temperature could be recorded by the corresponding equipment during the tests.

It is noteworthy that the SH and SAP coating surfaces are very difficult to be contaminated by artificial pollution slurry (e.g., diatomite and NaCl) as the widely reported pollution method in RTV system by brushing artificial pollution slurry, which is due to the excellent water repellency performance of the SAP and SH surfaces. Consequently, we developed a sieve method to simulate surface contamination for the flashover tests. Diatomite and NaCl were respectively used to simulate the insoluble substances and soluble salts in the contaminants. The slurry of diatomite and NaCl was dried and ground, and the resulting powder mixture was evenly sieved on the coatings with a 200# sieve by fixing non-soluble deposit density (NSDD) of 0.3 (light pollution grade), 0.6 (medium grade), and 0.9 mg/cm^2 (heavy grade) and salt deposit density (ESDD) of 0.05 (light grade), 0.10 (medium grade), and 0.15 mg/cm^2 (heavy grade), respectively. The specimen was fully exposed to a saturated moisture in a fog chamber for 15 min, and then the flashover test was performed on the specimen plate by the even-rising voltage method.

3 Result and discussion

3.1 Fabrication and characterization of SAP coatings

The hierarchical gradient micro-nanostructure in the present work is simply achieved by sequential spay-depositing a resin-based primer containing nylon particles and a topcoat containing silica NPs as-modified with low-surface-energy species (i.e., methyl groups or fluorocarbon groups). The successful modification of silica surface by grafting fluorocarbon groups can be confirmed by FTIR spectra and analyses (Figure S1), in which the absorption bands at 1204, 957, and 702 cm^{-1} are attributed to the C-F stretching vibration of the -CF_3 and -CF_2- groups in the fluorinated alkyl chains [42, 43]. The HRTEM

image and XRD pattern indicate that the as-synthesized silica are amorphous NPs in sphere-like shape (Figure S2). The microscale mastoid-like structure on the primer surface (Figure 1a) was formed by the atomization effect in the spraying process,[23] in which the introduction of nylon particle fillers played a critical role. The primer coating surface obtained in the absence of nylon particles is comparatively flat without any mastoid-like structure (Figure S3). Upon spray coating silica NPs on the nylon-absent primer, nanoporous structure and nanoscale roughness were observed (Figure S4), which is similar to that of previously reported SH silica-based coating directly deposited on substrate (i.e., without primer) [7, 44]. The formation of nanoscale silica particles (around 50 nm as-estimated by TEM image in Figure S2a) and microscale mastoid structure (verified by SEM image in Figure 1a) facilitates the formation of micro-nanoscale hierarchical architecture [45]. As detailed in Figure S5, large quantities of plateau-like microstructures are distributed on the surface of the primer in the presence of nylon particles. By subsequent spray-coating the silica-based layer, a conspicuous micro-nanoscale structure with a nanoscale roughness was formed (Figure 1b-c, e-f, and more details in Figures S6a-d and S7a-d), which was attributed to the decoration of silica NPs on the outer surface of the as-formed microscale mastoid-like structure of the primer. This hierarchical texture is critical to rendering a surface with excellent liquid repellency property. It is more interesting that a gradient structure was formed due to the interdiffusion between silica NPs and the resin-based primer, which can be verified by a cross-section SEM image and corresponding energy dispersive X-ray spectroscopy (EDS) mapping (Figure S8). The EDS analyses indicate that F, C, Si, and O are distributed in both the primer and topcoat. However, the concentration of C in the primer is much higher than that in the topcoat, which is attributed to the presence of resins and nylon particles. It is noteworthy that the concentration of Si gradually decreases from the topcoat to the bottom of the primer, suggesting that the distribution concentration of silica NPs decrease from the primer

to the primer-substrate interface (see again Scheme 1). These results reveal that some silica nanoparticles diffuse into the primer, resulting in the formation of a gradient structure. Although the spay-coating technique has been widely applied to fabricate SAP surfaces due to the great convenience and scalability [32, 34, 39, 40], we emphasize in our work that an appropriate spraying pressure (i.e., 2.0-2.5 bar in our work) and nozzle to substrate surface distance (i.e., 15-20 cm) played critical role in the fabrication of gradient structure. Furthermore, spaying silica NPs needs to be performed before the resin-based primer completely dries. All these deposition conditions facilitate the diffusion and tight interconnectivity of the silica NPs to the primer. The formation of gradient structure with strong interfacial connection plays a critical role in improving mechanical robustness and durability of the coating, which will be discussed later.

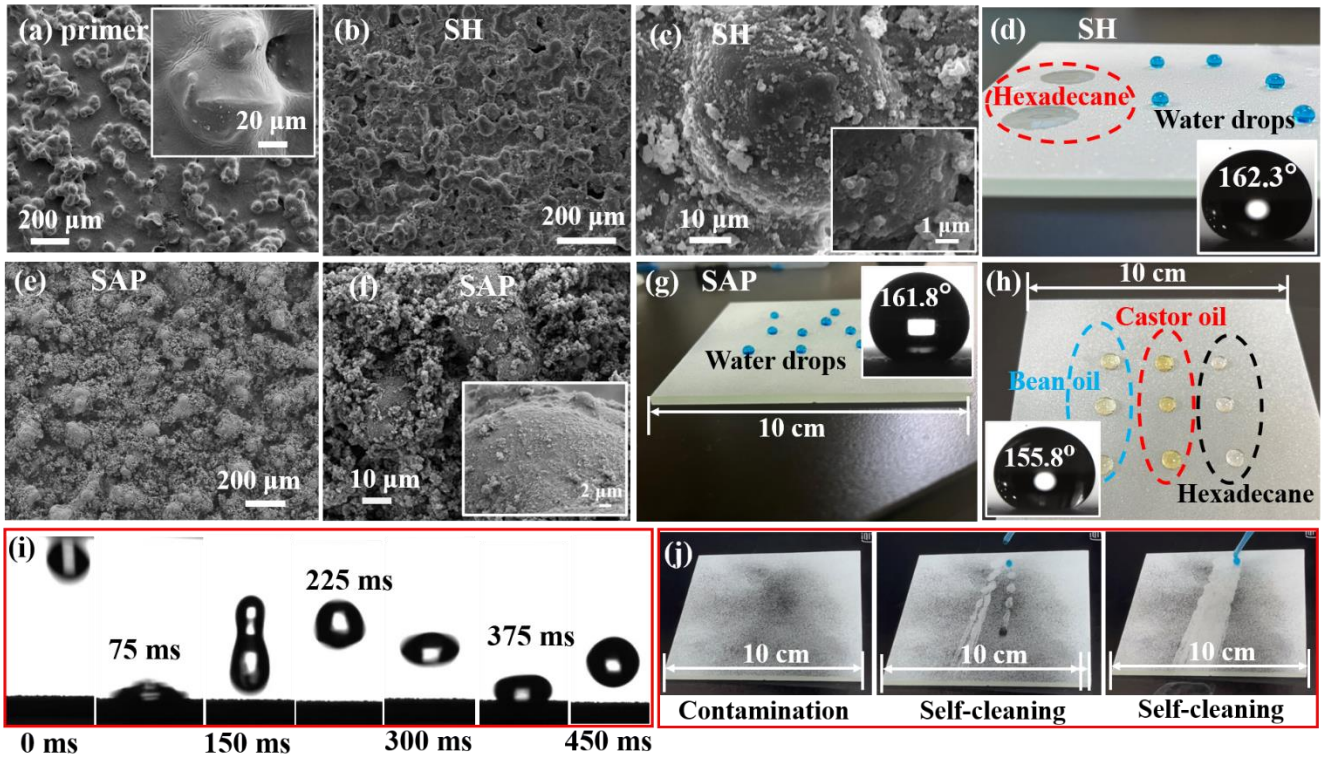

Figure 1 (a) SEM images of the primer showing mastoid morphologies of the surface. (b-c) SEM images of the SH coating displaying hierarchical micro-nano structure of the surface. (d) The surface superhydrophobicity of SH coating enables the spherical water droplets (dyed with methyl blue) resident on top, while oil drops completely spread on the surface. (e-f) SEM images of the SAP coating surface showing hierarchical micro-nanostructure. (g-h) The superoleophobicity and superhydrophobicity of the SAP coating enable the spherical dyed water droplets and organic droplets (e.g., bean oil, hexadecane, castor oil) resident on top. Insets in panels (a, c and f) provide the high-magnification SEM images of the corresponding surface. Insets in panels d) and g) provide the optical images of the resident water droplets on the corresponding coating when measure WCA. Inset in panel h) reports the optical image of the hexadecane droplets on the corresponding coating when measure OCA. (i) Water droplet (5 μL in volume) pinning and re-bouncing behaviour when released from a height of 2.5 mm toward the SAP surface. (j) Dropping dyed water on the fly-ash-contaminated SAP coating to display the self-cleaning performance of the SAP surface.

The wettability of the resin-based primer surface was different with that of "primer + topcoat" surface mainly due to the different chemical compositions. The hydrophobic-oleophilic (H-O) primer surface with WCA and OCA around 102^{o} and 31^{o} can be transformed to an SH surface with WCA exceeding 150^{o} and WRA below 10^{o} by spray-coating an additional methyl-modified silica-based layer (Figure 1d, and Figure S6f). The resident water droplets retain the spherical shapes however oil droplets (hexadecane) spread on the surface (identified by the red circles in Figure 1d). After depositing silica-based layer in which the surface of the silica NPs was modified by fluorocarbon molecules, both OCA and WCA on the surface exceeded 150^{o} while the WRA and OSA were below 10^{o} (Figure 1g-h, and Figure S7g-h),

indicating excellent SAP property of the as-fabricated coating. Water and oil droplets deposited on the surface adapt a spherical shape with WCA >160° and OCA >150°, respectively (Figure 1g-h).

Unlike many previously reported fabrication procedures of SH or SAP surfaces by using PFDTMS as surfactant [46-48], in our case, SAP coating cannot be obtained by spraying silica-based dispersion which formed in the absence of acid solution or even insufficient acid solution. This observation indicated that a sufficient acidification environment is critical for the surface modification of silica NPs by PFDTMS. We tried introducing various acid precursors such as H_2SO_4, HCl and HNO_3, and noticed that amount of H^+ ions (from acid solution) need to be much higher than that of OH^- ions (from NaOH) in order to finalize both superhydrophobicity and superoleophobicity.

It is of great interest that the excellent water- and oil-repellent properties of the SAP coating offer excellent self-cleaning performance, and contaminants can be removed from the surface by casting not only water droplets (Figure 1j, and Figure S9a-c) but also oil droplets (Figure S10a-c). As confirmed in Videos S1 and S2, water or pump oil droplets can easily roll down over the SAP coating, simultaneously taking away the contaminants (i.e., fly ash) and making the as-sainted surface clean. As a comparison, RTV surface displays no self-cleaning performance due to the low hydrophobic degree (Figure S9d-f, and Video S1), and dropping oil droplets cannot remove fly-ash powder from the SH surface due to the superlipophilicity (Figure S10d-f and Video S2). It is noteworthy that the motion behaviour of oil drops on SAP surface is different to that of water drops: the pump oil droplets slide from the SAP surface while water droplets roll off the surface (Video S3). This different motion behaviors of oil and water droplets on SAP surface is related to the different contact angle hysteresis of the corresponding liquids [49]. Consequently, we use “sliding angle” instead of “roll-off angle” to describe the tilting angle of the coated glass slides when the oil droplets slide down from the surface.

It was noticed that the surface wettability of the coatings can be controlled by tuning the amounts of hydroxyl acrylic resin (HAR) in the silica-based topcoat. Less silica NPs on the microscale mastoids were observed and the nanoscale roughness was not prominent with the increase of the HAR amount (Fig. S11). Concomitantly, the hydrophobicity and oleophobicity degrees decreased (insets in Figure S11b, d and f). Low degree of hydrophobicity and oleophobicity would lead to weakening flashover properties, which will be discussed later.

3.2 Stability and durability of the coatings

The stability and durability of coatings in outdoor applications, especially in some abnormal conditions such as the abrasion, exposure to sunlight, extreme temperature or corrosion environments are imperative issues [50]. However, these performances have not been fully explored in SAP or SH materials for improving flashover strength [22]. The sandpaper abrasion tests were carried out on the SAP surface to examine the mechanical robustness by following a previously reported method [43, 51]. The coated SAP glass slide of size 10 mm × 10 mm × 0.8 mm (under a 100 g load) was pushed to move on the sandpaper (grit size 800, 200 mm × 200 mm) at a constant slow speed (around 1 cm s^{-1}) for 10 cm to complete one abrasion cycle (Figure 2a). The coated side was touching the abradant and the SAP coating experienced a calculated pressure of 9.8 kPa (Figure 2a).

Figure 2b-c illustrates the evolution of the surface wettability over the abrasion cycles, which displayed that the coatings maintained superhydrophobicity even after 600th abrasion cycle, with WCA exceeding 150° and WRA below 10^{o} (Figure 2b). Although the values of OCA dropped down faster than those of WCA upon sandpaper abrasion, the OCA and OSA for pump oil on the coatings upon abrasion below 400 cycles still remained 151^{o} and <9^{o}, respectively (Figure 2c). These results confirmed that the SAP coatings can preserve their super water and oil repellency even if the surface was partially damaged. To

understand why the coatings is robust against abrasion, we further examined SEM images of the coatings after 200, 400, and 700 sandpaper abrasion cycles (Figure 2d-g, and Figure S12) and EDS mappings of the fresh SAP coating and 200th cycle coating (Figure S13). Compared to the original surface (Figure S12a-b), clear scratches on the skeleton surfaces of the coatings after sandpaper abrasion were observed (Figure 2d-g, and Figure S12c-h). The surface of the coating displayed breakage on the relatively big plateau-like microstructure after 200 cycles of abrasion, typically identified by the red dashes in the SEM image (Figure 2d-e). However, the main hierarchical micro-nanostructure of the skeleton in the coatings was well maintained thanks to the presence of nylon particles in the primer. Particularly, most of the silica NPs surrounded by the plateaux remained visibly intact and some small hill-like structures were preserved without damage after abrasion. With the increase of abrasion cycles, more spires of the mastoids were damaged and the surfaces were more flattened (Figure 2f-g).

The mechanism on the retention of SAP properties upon sandpaper abrasion is further shown in Figure 2h. The tips of the mastoid on the coating surface were scratched away upon abrasion and partial primer sections exposed to air and display locally hydrophobicity and lipophilicity due to the intrinsic H-O property of the resin-based primer (see again the Figure S4d-e). However, the overall micro-nanoscale skeleton was preserved and some intrinsically SAP silica NPs remained embedding in the as-scratched mastoid-like structure thanks to the formation of gradient structure. Furthermore, both the relatively small mastoids and the silica NPs surrounded by the big plateau-like microstructure were preserved without damage after abrasion. Indeed, EDS analyses indicate that the signals of Si, O, and F at the mastoid area (marked by dashed white circles in Figure S13a) are stronger than those at other areas on the fresh surface (i.e., without abrasion). Upon sandpaper abrasion, signals of Si, O, and F are still detected on the damaged mastoid (marked by dashed white circles in Figure S13g), but they became relatively weak

(Figure S13h-k). Besides, the atomic fractions of F, Si, and O on the surface decrease after abrasion in comparison with those of fresh coating (Figure S13f,l). These features reveal that the preservation of SAP performances upon repeated sandpaper abrasion stems from the micro-nanoscale mastoid-like structure and the unique gradient structure.

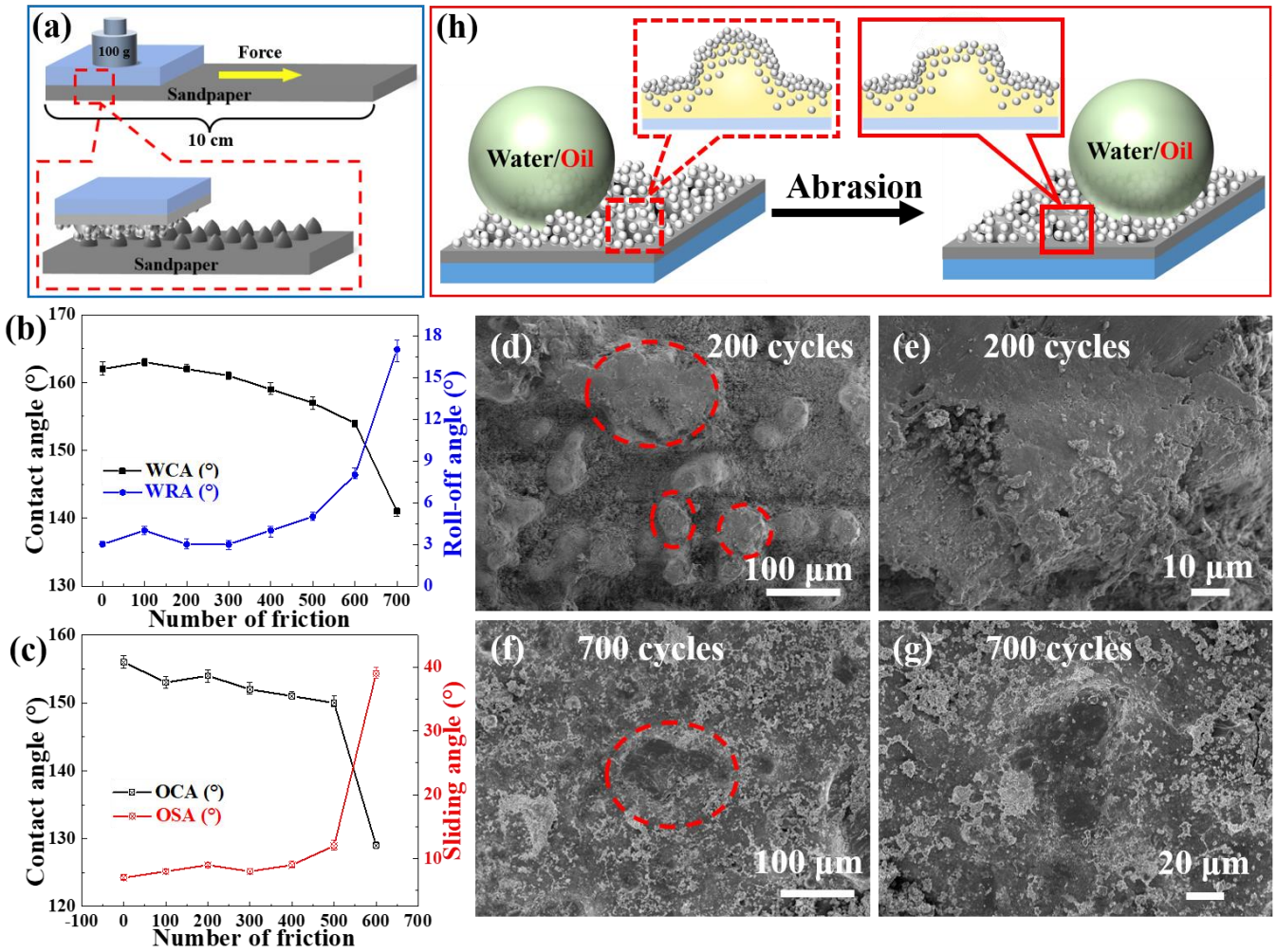

Figure 2 (a) The scheme illustrating the sandpaper abrasion test. (b-c) Evolution of WCA and WRA (a), OCA and OSA (b) on the SAP coatings over sandpaper abrasion cycles. The oil for OCA and OSA tests is pump oil. (d-g) SEM images of SAP coatings after sandpaper abrasion test for 200 cycles (d-e), and

700 cycles (f-g), respectively. (h) The mechanism on persistence of superamphiphobicity upon sandpaper abrasion.

The UV illumination stability and chemical stability of coatings are also crucial for outdoor applications. Figure 3a-b depicts the evolution of wettability of the representative coated SAP glass slides over UV illumination time, which indicates that the coating surface always maintained both superoleophobicity and superhydrophobicity even after 288 h of UV illumination. The coated SAP glass slides were also immersed in H_2SO_4 and NaOH solutions, respectively, with different pH values to examine the robustness under acid and alkaline environments. The values of the WCA and OCA could be preserved above 150^o and those of WRA and OSA were below 10^o after 168 h of immersion in the above solutions (Figure 3c-d). It was noticed that upon removing the SAP glass slides from the extreme corrosion solutions (e.g., pH = 1 and pH = 14 solutions, respectively) after continuous soaking for 168 h, the coating surface maintained nonwetting performance without adhesion of water droplets or water film (Videos S4). Both water and pump oil droplets could preserve spherical shape on the SAP coatings (Figure 3e-f). We also noticed that the super water- and oil-repellency capability of the SAP glass slides could be maintained after submersion in RT water for more than 5 months (not shown here), suggesting a stable long-term immersion performance.

Figure 3g-i further reports the stability of the SAP coatings under different temperatures. Interestingly, the coating exhibited WCA and OCA >150°, and WRA and OSA $<10^o$ even after they were treated at extreme temperatures ranging from -18^oC to 350^oC (see also Figure S14a-b). It was noticed that the color of the coating became light yellow at 200^oC and black at 350^oC (Figure S14c), which is due to the carbonization of resins in the primer. As shown in SEM images, microscale cracks were observed at 200^oC, and the size of the cracks increased at 350^oC. However, the surface maintained the overall

hierarchical micro-nanoscale structure, which explains the maintenance of super water- and oil-repellency performance. At higher temperature such as 400°C, the coating would peel off from the substrate and lose the SAP properties (not shown here).

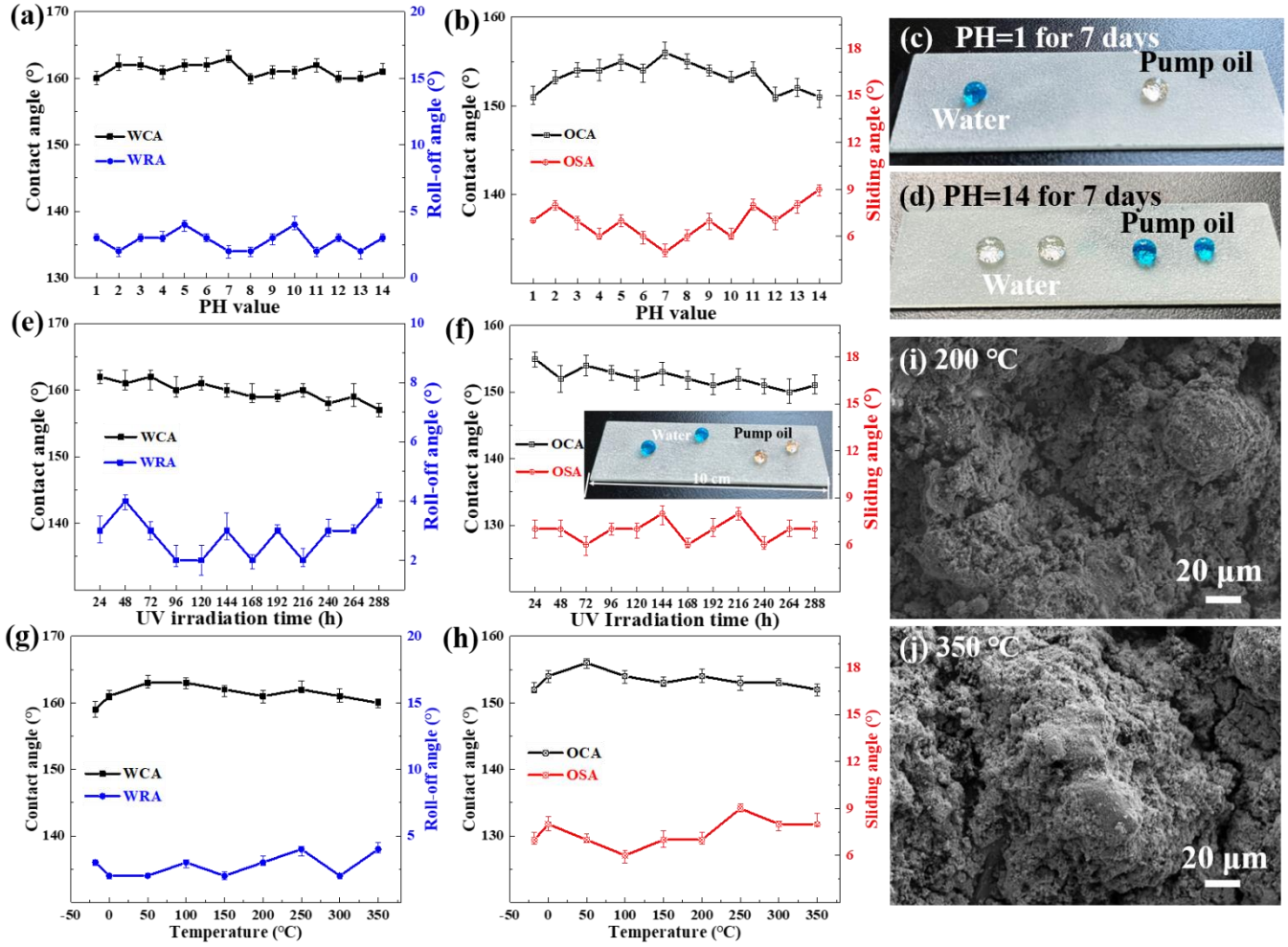

Figure 3 Chemical stability (a-d), UV irradiation stability (e-f)), and thermal stability (g-j) of the SAP coating. (a-b) The evolution of WCA, WRA (a) and OCA, OSA (b) of the coated SAP glass slides after having been soaked in solutions of different pH values for 168 h. (c-d) Digital photographs displaying that both water and pump oil droplets preserve sphere-like shape on the coatings collected after submersion in extreme corrosion solutions (e.g., pH = 1 and pH = 14 solutions, respectively) for 168 h. (e-f) The evolution of WCA, WRA (e) and OCA, OSA (f) of the coated SAP glass slides over UV

irradiation time. Inset in panel f) shows the digital photograph of the coating together with water and pump oil droplets after 288 h of UV irradiation. (g-h) WCA, WRA (g) and OCA, OSA (h) of SAP coating treated at different temperatures for 2 h. (i-j) SEM images of the SAP coatings treated at 200^{o}C and 350^{o}C, respectively, for 2 h.

The aforementioned results confirm that the SAP coatings possess excellent surface resistance to extreme environments such as repeated abrasion, corrosive chemicals, long-term UV radiation, and thermal degradation, which stems from the unique synergistic contribution of the unique gradient structure, the hierarchical architecture, the strong modification by PFDTMS, and the tightly inter-diffusion between resin-based primer and silica-based topcoat. The excellent stability and durability would be critical and promising in practical application such as anti-flashover of outdoor transmission line devices.

3.3 Pollution leakage current of various coatings on glass slides and evaluation model of pollution flashover

The pollution flashover tests of the uncoated glass slide, coated SAP and SH glass slides, and RTV-coated glass slide with sizes of 10 × 10 cm were performed in an artificial pollution flashover platform with a parallel electrode configuration under a rising DC voltage. Figure 4a reports the evolution of leakage current over applied DC voltage of the various coatings on glass slides after light pollution by contaminants (i.e., mixture of diatomite and NaCl), which indicates a linear relationship between the leakage current and DC voltage from 1 to 10 kV, by analogy to that of the previously reported SH coating [21]. At any voltage level below 10 kV, the leakage current of SAP coating surface is almost the same as that of SH surface (see also the enlarge view of the curves in Figure S15), but much less than the leakage

current of RTV-coated and uncoated surfaces. Correspondingly, the leakage current growth rate of SAP and SH surfaces is much smaller than that of RTV and uncoated surfaces (Table S1), which is consistent with the previously-reported comparison of leakage current between SH and RTV surfaces [21]. We also noticed that the hydrophobicity and oleophobicity strength affects the flashover properties, which is confirmed by the fact that the leakage current of H-O surfaces is much higher than that of SH and SAP surfaces at any voltage level. For more prominent comparison, the sample with WCA of 141^{o} displayed much lower leakage current (blue curve in Figure 4a) than that of sample with WCA of 121^{o} (green curve in Figure 4a). The enhancement of the hydrophobicity would reduce the effective solubility of soluble salt and the maximum value of local surface conductivity, and thus improves the flashover strength [52]. Besides, at any voltage level, the leakage current increased with increasing pollution grade (Figure 4b). As the voltage was increased, the leakage current of SAP coating surface displayed a ramp increment at 35, 38 and 40 kV under heavy, medium, and light pollution, respectively (Figure 4b). These observations indicate that the pollution flashover performance was weakened with the increase of pollution grade. The detailed comparison on leakage current of the representative specimens under 10 kV and various pollution conditions (i.e., heavy, medium, and light pollution grade, respectively) is further reported in Figure 4c, further confirming that the leakage current of SAP coating is much lower than that of all other specimens.

The prominent difference of the pollution flashover properties of the various coatings is due to the different surface wettability and self-cleaning property. Normally, water droplets cannot easily adhere on the SAP and SH surfaces and thus the contaminants are easily removed from the surfaces, which improves the pollution flashover strength. Small liquid droplets containing water and pollutants were observed on all the above-mentioned coatings after being contaminated and exposed to a saturated

moisture environment for 15 min. However, the numbers of the droplets on SAP and SH surface were much less than those on uncoated and RTV-coated glass slide (Figure 4d-f, and Figure S16). The presence of water droplets can reduce the insulation path and thus lead to the weakening flashover strength. These results explain why the SAP and SH coatings displayed much lower leakage currents as compared with RTV coating.

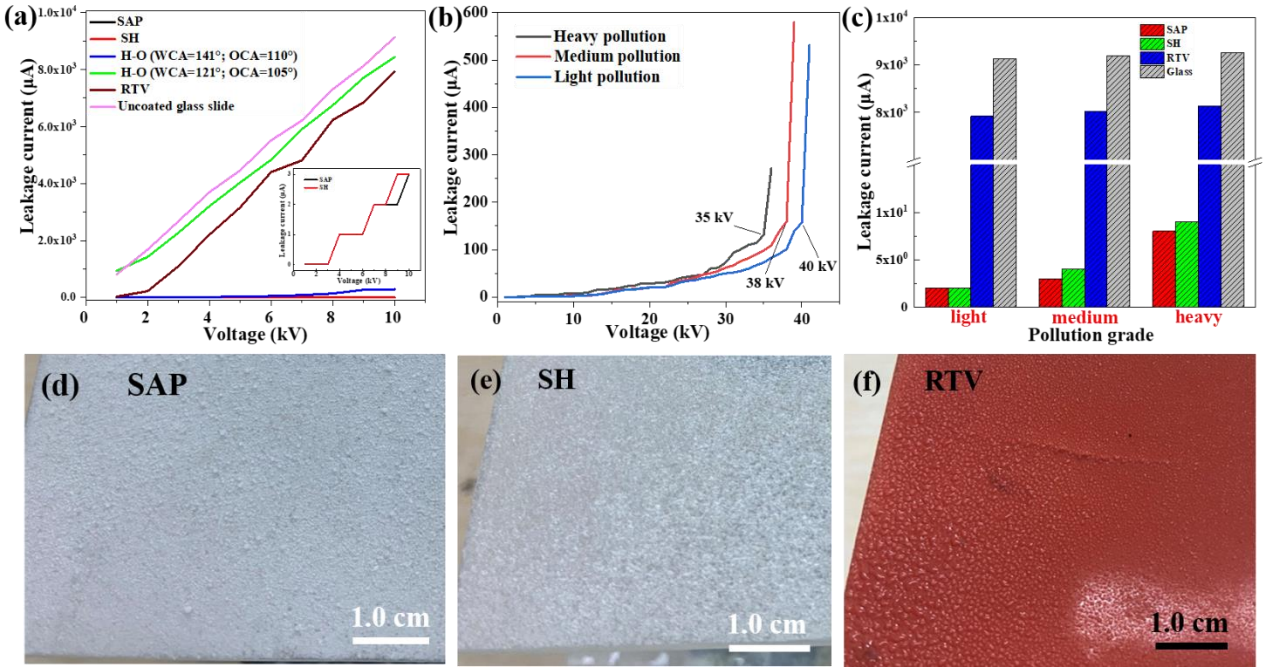

Figure 4 (a) Experimental measurement curve of leakage current and DC voltage of the various coatings under light pollution environment. Inset provides the enlarge view of the curve regarding SAP and SH coatings. (b) Experimental measurement curve of leakage current and DC voltage of the SAP coating under three levels, namely heavy, medium, and light contamination. (c) The column chart of leakage currents of various specimens as dictated under 10 kV of DC voltage and heavy, medium and light pollution environment, respectively. (d-f) Digital photographs of SAP (d), SH (e) and RTV (f) coatings after contamination by diatomite powders and wetting in the fog chamber.

The process of insulator flashover under wet conditions is composed of several stages, namely wetting, formation of dry bands, dry band arcing, propagation of dry band arcing and flashover. Most flashover models including those of extensively studied hydrophobic RTV-based insulator system were derived from the Obenaus model. Huang and co-workers established a model to describe the pollution flashover process on a hydrophobic surface according to the Kirchhoff laws [25]:

$$U = U_{arc} + U_p + mU_{ac} \quad (1)$$

where U is the applied voltage during flashover. U_{arc}, U_p and U_{ac} are the voltage of the arc, the voltage of the residual contamination layer and the voltage of the droplet, respectively. m is the number of partial arcs in the discharge channel.

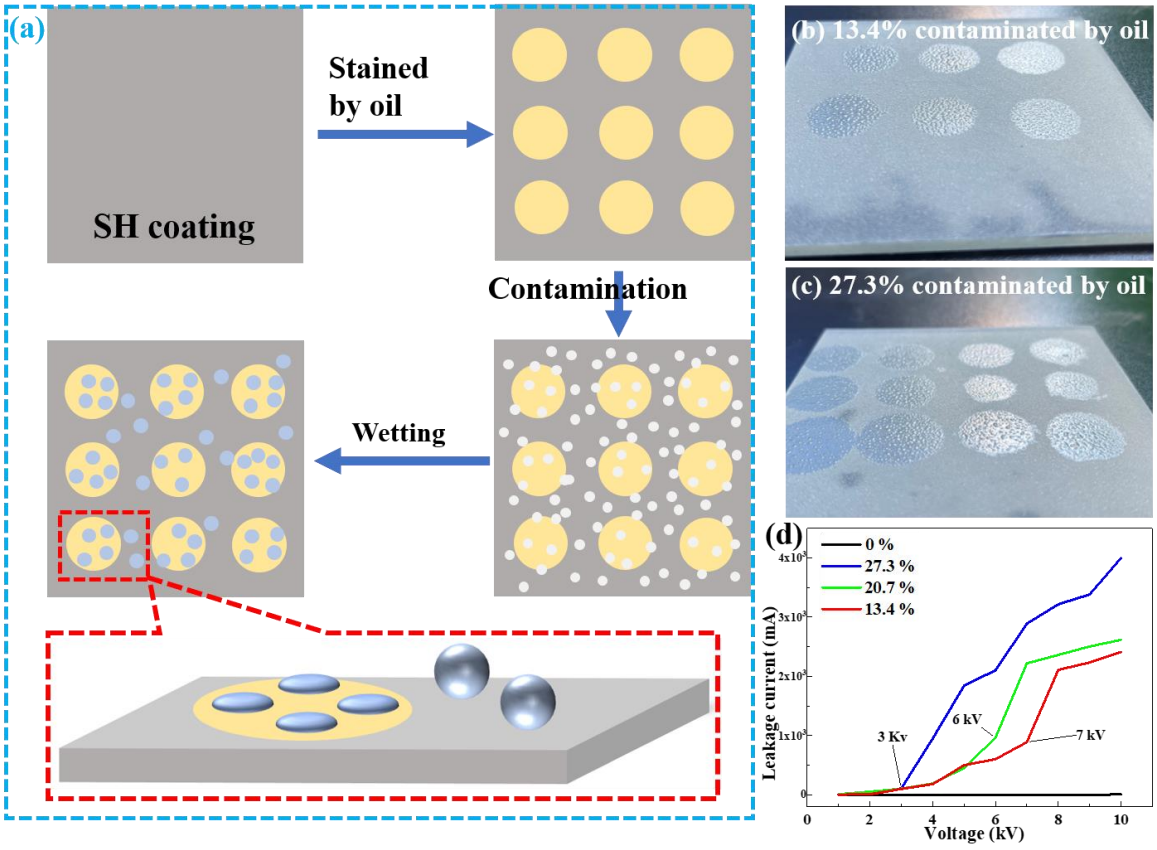

Figure 5 (a-c) Scheme illustrating the evaluation proposal for pollution flashover upon organic contamination. (d-e) The digital photographs of the SH coatings after contamination by different drops of hexadecane and exposing to saturated moisture environment. (f) Experimental measurement curve of leakage current and DC voltage of the SH coating after contamination by hexadecane droplets and diatomite powder.

We emphasize that organic contamination cannot be completely avoided in outdoor applications [27, 28]. Oil droplets with surface energy lower than that of surfactant species (e.g., methyl groups) on coating or NP surface might spread on the SH surfaces (RTV surface as well), which has been verified in our work (e.g., Figure 1d). We further noticed that ambient dust easily adheres on the surface that was locally contaminated by organics (simulated by hexadecane droplets in our work) in comparison with the uncontaminated place when the specimens (e.g., SH insulator) were put outdoors for some time (e.g., two months). In this case, droplets of contaminants or even large-area wetted contaminants would form on the organic-stained places under moisture environment, which would affect flashover strength. Consequently, the influence of organic contamination on the pollution flashover performances needs to be considered. We thus propose a model to evaluate the pollution flashover performances in which the influence of organic contamination is included. To simplify the discussion, we presumed that the organic-stained place of the surface was further contaminated by dust pollutants (simulated by mixture of diatomite and NaCl in our work), which was then wetted in a saturated moisture environment (Figure 5a). The modified model to describe the pollution flashover process on an SH or hydrophobic surface can be then proposed as follows:

$$U = U_{arc} + U_p + U_{p-org} + mU_{ac} \quad (2)$$

where $U_{p\text{-}org}$ is the voltage of the residual contamination layer of the organic-stained place. One can deduce from equation (2) that the replacing of an originally SH surface by an organic-contaminated area would be easily contaminated by other environmental pollutants (e.g., dusts) and wetted under moisture environment, which would lead to the weakening insulation strengthand pollution flashover performance [53].

Experimentally, we choose three coated SH glass slides with the same size (i.e., 10 × 10 cm) and cast different numbers of hexadecane droplets on each slide to evaluate the influence of organic contamination area on the pollution flashover properties. The experimental area percentage of the organic contamination relative to the whole SH surface are estimated to be 13.4%, 20.7% and 27.3%, respectively (Figure 5b-d). Simulated contaminant (i.e., mixture of diatomite and NaCl) was evenly sieved on the SH surface, followed by exposing to a saturated moisture environment for 15 min. We observed that the amount of droplet containing both water and powder at the oil-stained place was much larger than that at other place (Figure 5b-c). This experimental observation further verified our presumption that oil-stained area of a SH surface was easily adhered by dust and wetted under a moisture environment. The flashover test of the stained and wetted specimens was then performed and the results are reported in Figure 5d. Overall, at any voltage level, the leakage current of the SH coating with less organic-contaminated area was lower than that of SH coating with larger contamination area. It is noteworthy that hexadecane droplets cannot easily adhere on the SAP surface due to its excellent oil repellency. Consequently, the leakage current of the SAP surface after casting hexadecane droplets on it was almost the same as the fresh SAP surface (dark curve in Figure 5d), which was much lower than that of an oil-contaminated SH surface. We also need to point it out that the pollutants of organic and dust in a real-world ambient environment are varied, which would lead to the variation of the amount of water adhered on the organic-contaminated place

under harsh environment, and the amount and conductivity of water droplets would affect the flashover performance [26]. Furthermore, the dielectric constants of water, organic pollutants, and dusts are different, which complicates the in-depth discussion on $U_{p\text{-}org}$ in the equation (2). Hence, it is difficult to establish an exact quantitative relationship between the organic contamination and the pollution flashover strength at present.

3.4 Self-cleaning and pollution flashover performance of coated insulators

It can be concluded from the above-discussed results that the enhanced pollution flashover performances of a surface stem from its improved water and organic repellency and self-cleaning properties. We thus fabricated various coated glass insulators (i.e., RTV, SAP and SH insulators) and studied their anti-fouling, self-cleaning and anti-flashover performances. First, the spraying-coated SAP glass insulator was immersed in RT water for 60 days and lifted out from the water to check its wettability (Video S5). The SAP insulator was completely dry when lifting it from the water, confirming an excellent water repellency. However, water films were formed on RTV-coated glass insulator, even after soaking in water for few seconds (Video S5). Second, the wettability of the insulators was studied in a simulated raining environment (Video S6). The flowing water was scattered on the coated SAP and SH insulators and rolled down from the surface, offering a completely dry surface after stopping the stimulated rain. However, water droplets gathered to form a water film on the surfaces of uncoated or RTV-coated glass insulators, and water continuously flowed down. Upon stopping the rain, a water film and many water droplets adhered on the uncoated and RTV surfaces. Finally, self-cleaning experiments were performed by contaminating the SAP and RTV surfaces with fly-ash powders and purifying by the dropping water (Videos S7 and Figure S17). Contaminants can be easily removed upon water droplets rolling on SAP surface, making the surface clean (Figure S17a-c). In comparison, water droplets adhered on the RTV

surface due to the low hydrophobicity of the surface and the surface kept dirty (Figure S17d-f). All these results undoubtedly confirm the excellent self-cleaning ability and anti-contamination behavior of the SAP coatings, which would facilitate enhancing the pollution flashover performance and will be discussed in the following sections.

The tests of pollution flashover were conducted in an artificial pollution flashover platform, under ambient atmosphere conditions. The applied AC voltage on the specimens was gradually raised until the flashover happened, from which the pollution flashover (PFOV) was estimated. First, the PFOVs of the various representative insulators under light pollution level are compared in Figure 6a, indicating that the coated SAP and SH glass insulators presented stronger pollution flashover strength in comparison with H-O and RTV-coated glass insulators. For example, the PFOVs of SAP and SH specimens under light pollution environment were 73.363 and 68.795 kV (Figure 6a), respectively, which were 29.0% and 20.9% higher that that of the RTV-coated insulator (i.e., 56.883 kV). Second, the pollution flashover property of SAP and RTV insulators under different pollution grades is reported in Figure 6b. In any grade, the PFOVs of SAP insulator was much higher than those of RTV-coated insulator. For example, under the heavy pollution grade, the PFOV of SAP sample demonstrated a 42.9% pollution flashover improvement compared to that of the RTV insulator. Table S2 provides the comparison of the synthesis methods and flashover performance of our specimens and the representative previously-reported SH samples, further confirming the excellent flashover stremgth of SAP coating. Figure 6b also demonstrates that the PFOVs of SAP and RTV-coated glass insulators decreased with increasing pollution grades from light, medium, to heavy. This trend is consistent with that of previously reported RTV sample [2]. The SAP insulator always displayed excellent anti-flashover performance, with only a slight decrease of the PFOV from 73.363 to 71.996 kV (i.e., 1.9% decreased PFOV) as the pollution grade increased from light to heavy. In

contrast, a RTV-coated sample showed larger decrease from 56.883 to 50.38 kV, that is, a 11.4% lower pollution flashover voltage with the the growing extent of pollution. Finally, it was noticed that the PFOV of the specimen without contamination is higher than that of specimen contaminated by mixture of diatomite and NaCl. For instance, PFOVs of SAP and RTV-coated insulator was detected to be 91.2 kV and 81.3 kV, respectively (not shown in the Figures). All these results confirm that fabricating SAP surface facilitates retaining good insulation strength and thus enhanced the anti-pollution flashoverper performance at any pollution levels.

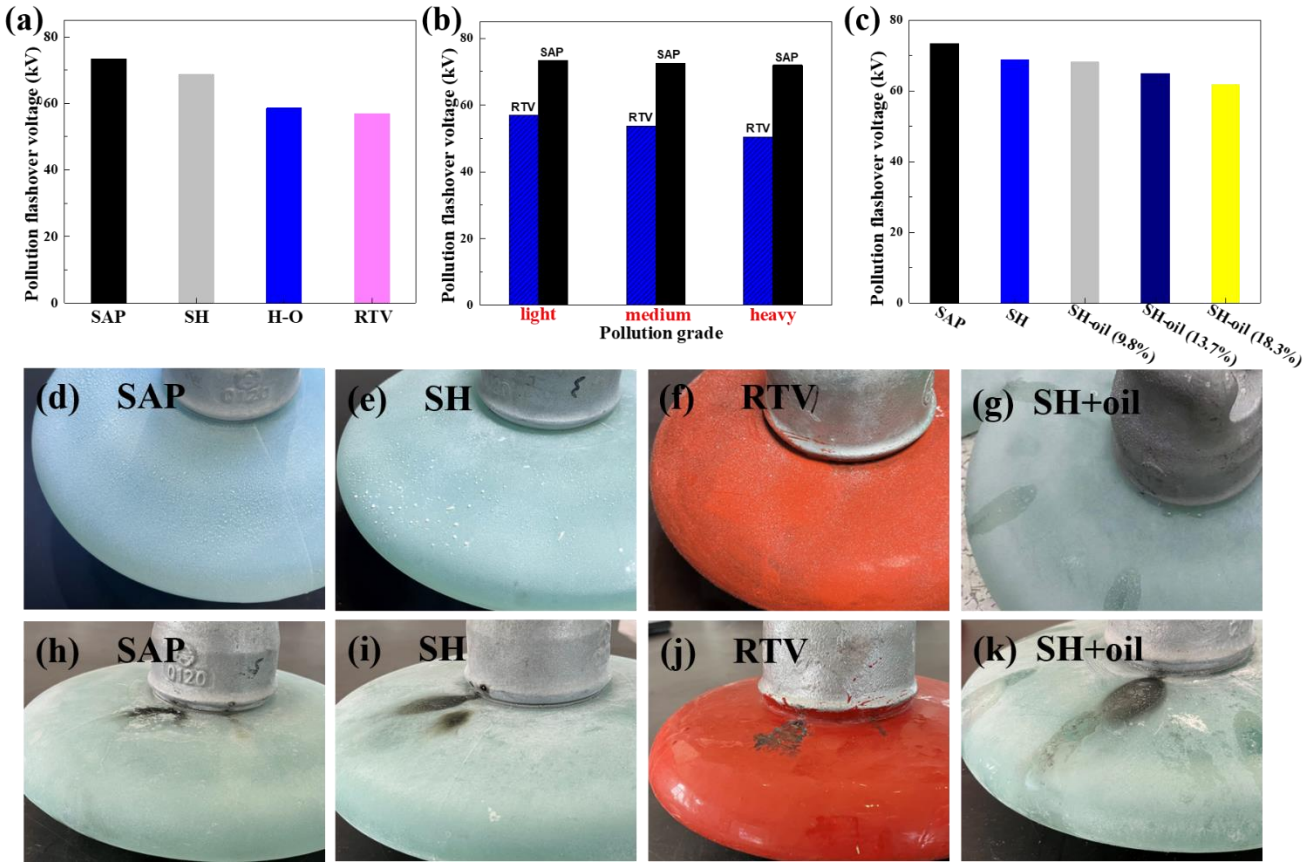

Figure 6 (a) The PFOVs of various insulators (SAP, SH, H-O and RTV represent coated SAP, SH, hydrophobic-oleophobic, and RTV-coated glass insulators, respectively). (b) PFOVs the SAP and RTV glass insulators under light, medium and heavy pollution grade, respectively. (c) PFOVs of the

representative oil-contaminated insulators (i.e., hexadecane droplets). (d-f) Digital photographs of the corresponding insulators after contamination by mixture of diatomite and NaCl, followed by exposing to saturated moisture environment. (g) Digital photograph of SH glass insulator contaminated by both simulated contaminants (i.e., mixture of diatomite and NaCl) and oil (i.e., hexadecane drops), followed by exposing to saturated moisture environment for 15 min. (h-k) Digital photograph of the various corresponding insulators after pollution flashover tests.

The influence of the water volume and number on the flashover property has been investigated [26]. We observed many small droplets containing water and particles of contaminants on all the related insulators after exposing to a saturated moisture environment for 15 min (Figure 6d-g). The amount of the wetted droplets on SAP and SH surfaces was much lower than that on RTV-coated insulators (see also Figure S18). The above different surface state is due to the different levels of water repellency between SAP insulator surface and RTV-coated surface. Low water adhesion and excellent water repellency on SAP surface facilitate the roll-off of water droplets and enlarge the clean area on the surface. This performance leads to longer insulation path and promotes the insulation strength in comparison with a hydrophilic or normal hydrophobic surface[26, 53], thereby leading to improvement of pollution flashover strength of the SAP coating. Additionally, higher surface roughness of the SAP (SH as well) surface than that of RTV surface extends the surface discharge path and hinders the development of electron avalanche, also playing a role in the increase of PFOV [20, 54].

To our knowledge, the flashover property of SAP coating has not been reported yet although SH surfaces have aroused great interest in improving flashover strength. Since organic contamination might occur in practical application, we chose three SH glass insulators and stained them with different amounts of hexadecane droplets and investigated the pollution flashover strength. By changing the numbers of the

hexadecane droplets (0.05 mL for each droplet) on the insulator surface, the percentage of organic-contaminated area relative to the whole insulator surface area were estimated to be 9.8%, 13.7% and 18.3%, respectively (Figure 6c). As shown in Figure 6c, compared with the original SH glass insulator (i.e., insulator without hexadecane contamination), 0.8%, 5.7% and 10.1% decrease in PFOV were noticed on the hexadecane-stained SH insulators with a contamination area of 9.8%, 13.7% and 18.3%, respectively. This observation undoubtedly revealed that organic contamination led to the weakening pollution flashover strength of the SH coating, futher confirming the influence of the $U_{p\text{-}org}$ fraction as-depicted in equation (2). For comparison, hexadecane droplets can easily slide out from the SAP insulator surface without visible oil contamination (Video S8), and thus have little effect on the PFOV. All these results indicate that the presented SAP coating is eminently suitable for improving pollution flashover performances of insulators in practical applications.

4 Conclusions

In summary, SAP coatings with gradient micro-nanoscale structure and excellent pollution flashover properties were fabricated by a facile and scalable spray-depositing “primer + topcoat” technique. The as-fabricated super liquid-repellent coatings displayed excellent performances such as self-cleaning capability, strong abrasion resistance, thermostability at extreme temperatures between -20^{o}C and 350^{o}C, UV radiation stability for 288 h, and resistance against soaking in extreme corrosion solutions (pH values between 1.0 and 14.0) for 168 h. The strong robustness and excellent durability can be ascribed to the synergistic contribution of the incorporation of the unique gradient structure, hierarchical textures, strong modification by fluorocarbon species, and the tight inter-diffusion between resin-based primer and silica-based topcoat. The excellent liquid repellency and self-cleaning properties of the surface endow the coated SAP glass slides and insulator with enhanced pollution flashover strength in comparison with that

of uncoated and RTV-coated specimens. The coated SAP glass insulator demonstrated 29.0% and 42.9% PFOV improvement than RTV-coated insulator under light and heavy pollution grade, respectively. Particularly, an evaluation model based on organic contamination for flashover strength was proposed and verified by experimental PFOV tests. The organic contamination on SH surface leads to the weakening of the pollution flashover strength, while the SAP coating allowed the retention of its flashover strength thanks to the excellent oil repellency. We believe that the presented protocol will provide a novel insight for fabricating unique and robust liquid-repellent surfaces, which would not only improve flashover strength in transmission line insulator system but also reveal other prospective outdoor applications.

Acknowledgments

This work is supported by the project “Synthesis and Application of Superhydrophobic Self-cleaning Materials for Electric Engineering” (No. 6111901321), Overseas Expertise Introduction Project (111 project) for Discipline Innovation of China (Grant No. B18038), and the State Key Laboratory of Silicate Materials for Architectures (Wuhan University of Technology) Open Foundation (Grant no. SYSJJ2021-02).

Electronic Supplementary Material: Supplementary material (SEM images, XRD pattern, digital photographs of contact angles, contact angle and sliding angle curves, self-cleaning test, energy dispersive X-ray spectroscopy (EDS) elemental mapping and EDS analyses, and digital photographs of the various coatings) is available in the online version of this article.

References

[1] Sarathi, R.; Danikas, M. RTV silicone rubber coatings for outdoor insulators: a concise review of some factors affecting their behavior and some comments. *J. Eng. Sci. Technol. Rev.* **2021**, *14*, 163-169.

[2] Ravindran, M.;Karuppiah, N.;Asokan, M.; Kumar, S. S. Experimental investigation on room temperature vulcanised silicone rubber and epoxy resin coated porcelain outdoor insulators

located at highly polluted environment. *J. Ceram. Process. Res.* **2020**, *21*, 14-20.

[3] Su, H.;Jia, Z.;Guan, Z.; Li, L. Durability of RTV-coated insulators used in subtropical areas. *IEEE Trans Dielectr Electr Insul* **2011**, *18*, 767-774.

[4] Zhang, Z.;Qiao, X.;Xiang, Y.; Jiang, X. Comparison of surface pollution flashover characteristics of RTV (room temperature vulcanizing) coated insulators under different coating damage modes. *IEEE Access* **2019**, *7*, 40904-40912.

[5] Phillips, A. J.;Childs, D. J.; Schneider, H. M. Aging of nonceramic insulators due to corona from water drops. *IEEE Trans. Power Deliv.* **1999**, *14*, 1081-1089.

[6] Zhu, Y.;Haji, K.;Yamamoto, H.;Miyake, T.;Otsubo, M.;Honda, C.;Kaikake, K.; Sugamoto, K. A Study on hydrophobicity of silicone rubber exposed to corona discharge. In *IEEE 8th International Conference on Properties & applications of Dielectric Materials*, 2006; pp 587-590.

[7] Kareem, S.;Xie, Y.;Li, T.;Ding, Y.;Tsiwah, E. A.;Ahmed, A. S. A.;Chen, J.;Qiao, F.;Chen, Z.; Zhao, X. Base-catalyzed synthesis of superhydrophobic and antireflective films for enhanced photoelectronic applications. *J. Mater. Res. Technol.* **2020**, *9*, 3958-3966.

[8] Xiong, W.;Li, L.;Qiao, F.;Chen, J.;Chen, Z.;Zhou, X.;Hu, K.;Zhao, X.; Xie, Y. Air superhydrophilic-superoleophobic SiO_2-based coatings for recoverable oil/water separation mesh with high flux and mechanical stability. *J. Colloid Interface Sci.* **2021**, *600*, 118-126.

[9] Liu, J.;Ye, L.;Sun, Y.;Hu, M.;Chen, F.;Wegner, S.;Mailänder, V.;Steffen, W.;Kappl, M.; Butt, H. J. Elastic Superhydrophobic and Photocatalytic Active Films Used as Blood Repellent Dressing. *Adv. Mater.* **2020**, *32*, 1908008.

[10] Zhao, X.;Wei, J.;Li, B.;Li, S.;Tian, N.;Jing, L.; Zhang, J. A self-healing superamphiphobic coating for efficient corrosion protection of magnesium alloy. *J. Colloid Interface Sci.* **2020**, *575*, 140-149.

[11] Li, Y.;Zhao, Y.;Lu, X.;Zhu, Y.; Jiang, L. Self-healing superhydrophobic polyvinylidene fluoride/Fe_3O_4@polypyrrole fiber with core–sheath structures for superior microwave absorption. *Nano Res.* **2016**, *9*, 2034-2045.

[12] Zhou, P.;Yu, H.;Zhong, Y.;Zou, W.;Wang, Z.; Liu, L. Fabrication of waterproof artificial compound eyes with variable field of view based on the bioinspiration from natural hierarchical micro-nanostructures. *NanoMicro Lett* **2020**, *12*, 166.

[13] Haghanifar, S.;McCourt, M.;Cheng, B.;Wuenschell, J.;Ohodnicki, P.; Leu, P. W. Creating glasswing butterfly-inspired durable antifogging superomniphobic supertransmissive, superclear nanostructured glass through Bayesian learning and optimization. *Mater. Horizons* **2019**, *6*, 1632-1642.

[14] Tzianou, M.;Thomopoulos, G.;Vourdas, N.;Ellinas, K.; Gogolides, E. Tailoring Wetting Properties at Extremes States to Obtain Antifogging Functionality. *Adv. Funct. Mater.* **2021**, *31*, 2006687.

[15] Bu, Y.;Shen, T.;Yang, W.;Yang, S.;Zhao, Y.;Liu, H.;Zheng, Y.;Liu, C.; Shen, C. Ultrasensitive strain sensor based on superhydrophobic microcracked conductive $Ti_3C_2T_x$ MXene/paper for human-motion monitoring and E-skin. *Sci. Bull.* **2021**, *66*, 1849-1857.

[16] Che, P.;Liu, W.;Chang, X.;Wang, A.; Han, Y. Multifunctional silver film with superhydrophobic and antibacterial properties. *Nano Res.* **2016**, *9*, 442-450.

[17] Hu, Y.;Kareem, S.;Dong, H.;Xiong, W.;Tian, S.;Shamsi, J.;Li, L.;Zhao, X.; Xie, Y. $CsPbBr_3$@SiO_2 core-shell nanoparticle films for superhydrophobic coatings. *ACS Appl. Nano Mater.* **2021**, *4*, 6306-6315.

[18] Jin, H.;Jin, P.;Niu, R.;Li, Y.;He, B.;Gao, N.; Zhang, H. Flashover characteristics of discrete water droplets on the surface of super-hydrophobic silicone rubber. *IEEE Trans Dielectr Electr Insul* **2014**, *21*, 1718-1725.

[19] Arshad;Momen, G.;Farzaneh, M.; Nekahi, A. Properties and applications of superhydrophobic coatings in high voltage outdoor insulation: A review. *IEEE Trans Dielectr Electr Insul* **2017**, *24*, 3630-3646.

[20] Wang, C.;Li, W.;Jiang, Z.;Yang, X.;Sun, G.; Zhang, G. UV-cured nanocomposite coating for surface charging mitigation and breakdown strength enhancement: exploring the combination of surface topographical structure and perfluorooctyl chain. *RSC Adv.* **2020**, *10*, 16422-16430.

[21] Chen, J.;Chen, J.;Li, L.;Wang, S.; Xie, Y. Study on the self-cleaning phenomenon and anti-pollution flashover performance of micro-nanostructure superhydrophobic coating surface under a high humidity environment. *Colloids Surf. A Physicochem. Eng. Asp.* **2021**, *630*, 127552.

[22] de Santos, H.; Sanz-Bobi, M. Á. Research on the pollution performance and degradation of superhydrophobic nano-coatings for toughened glass insulators. *Electr. Power Syst. Res.* **2021**, *191*, 106863.

[23] Zhu, M.;Song, H.;Li, J.;Xue, J.;Yu, Q.;Chen, J.; Zhang, G. Superhydrophobic and high-flashover-strength coating for HVDC insulating system. *Chem. Eng. J.* **2021**, *404*.

[24] Vallabhuneni, S.;Movafaghi, S.;Wang, W.; Kota, A. K. Superhydrophobic coatings for improved performance of electrical insulators. *Macromol Mater Eng* **2018**, *303*.

[25] Xu, W.;Niu, J.;Tian, K.;Huang, Z.;Li, J.;Wang, F.;Wei, Y.; Zhao, Y. Enhanced pollution flashover of a slurry coalescence superhydrophobic coating. *IEEE Trans Dielectr Electr Insul* **2021**, *28*, 310-317.

[26] Li, Y.;Jin, H.;Nie, S.;Zhang, P.; Gao, N. Dynamic behavior of water droplets and flashover characteristics on a superhydrophobic silicone rubber surface. *Appl. Phys. Lett.* **2017**, *110*.

[27] Bagali, H. S.;Shaik, S. A.; P, N. Insulator contamination in transmission lines. *IJERT* **2015**, *3*, 1-8.

[28] Hadipour, M.; Shiran, M. A. Various pollutions of power line insulators. *Majlesi J. Electr. Eng.* **2017**, *6*, 29-38.

[29] Chu, Z.; Seeger, S. Superamphiphobic surfaces. *Chem. Soc. Rev.* **2014**, *43*, 2784-2798.

[30] Lian, Z.;Xu, J.;Wang, Z.;Weng, Z.;Wan, Y.;Zhang, L.; Yu, H. Research on HS-WEDM and chemical etching technology of superamphiphobic surfaces on Al substrates. *Iet Micro & Nano Letters* **2016**, *11*, 425-429.

[31] Wang, H.;Zhang, Z.;Wang, Z.;Liang, Y.;Cui, Z.;Zhao, J.;Li, X.; Ren, L. Multistimuli-responsive microstructured superamphiphobic surfaces with large-range, reversible switchable wettability for oil. *ACS Appl. Mater. Interfaces* **2019**, *11*, 28478-28486.

[32] Wang, T.;Lv, C.;Ji, L.;He, X.; Wang, S. Designing re-entrant geometry: construction of a superamphiphobic surface with large-sized particles. *ACS Appl. Mater. Interfaces* **2020**, *12*, 49155-49164.

[33] Teisala, H.;Geyer, F.;Haapanen, J.;Juuti, P.;Mäkelä, J. M.;Vollmer, D.; Butt, H.-J. Ultrafast processing of hierarchical nanotexture for a transparent superamphiphobic coating with extremely low roll-off angle and high impalement pressure. *Adv. Mater.* **2018**, *30*, 1706529.

[34] Wang, K.;Liu, X.;Tan, Y.;Zhang, W.;Zhang, S.;Li, J.; Huang, A. Highly fluorinated and hierarchical HNTs/SiO_2 hybrid particles for substrate-independent superamphiphobic coatings. *Chem. Eng. J.* **2019**, *359*, 626-640.

[35] Zhou, H.;Wang, H.;Niu, H.;Zhao, Y.;Xu, Z.; Lin, T. A waterborne coating system for preparing robust, self-healing, superamphiphobic surfaces. *Adv. Funct. Mater.* **2017**, *27*, 1604261.

[36] Han, X.;Peng, J.;Jiang, S.;Xiong, J.;Song, Y.; Gong, X. Robust Superamphiphobic Coatings Based on Raspberry-like Hollow SnO_2 Composites. *Langmuir* **2020**, *36*, 11044-11053.

[37] Zhou, H.;Wang, H.;Niu, H.;Fang, J.;Zhao, Y.; Lin, T. Superstrong, chemically stable,

superamphiphobic fabrics from particle-free polymer coatings. *Adv. Mater. Interfaces* **2015**, *2*, 1400559.

[38] Lu, Y.;Sathasivam, S.;Song, J.;Crick, C. R.;Carmalt, C. J.; Parkin, I. P. Robust self-cleaning surfaces that function when exposed to either air or oil. *Science* **2015**, *347*, 1132-1135.

[39] Wei, J.;Li, B.;Jing, L.;Tian, N.;Zhao, X.; Zhang, J. Efficient protection of Mg alloy enabled by combination of a conventional anti-corrosion coating and a superamphiphobic coating. *Chem. Eng. J.* **2020**, *390*, 124562.

[40] Jiao, X.;Li, M.;Yu, X.;Wong, W. S. Y.; Zhang, Y. Oil-immersion stable superamphiphobic coatings for long-term super liquid-repellency. *Chem. Eng. J.* **2021**, *420*, 127606.

[41] Zhu, Q.;Li, B.;Li, S.;Luo, G.;Zheng, B.; Zhang, J. Durable superamphiphobic coatings with high static and dynamic repellency towards liquids with low surface tension and high viscosity. *J. Colloid Interface Sci.* **2020**, *578*, 262-272.

[42] Guo, C.;Ding, H.;Xie, M.;Zhang, H.;Hong, X.;Sun, L.; Ding, F. Multifunctional superamphiphobic fluorinated silica with a core-shell structure for anti-fouling and anti-corrosion applications. *Colloids Surf. A Physicochem. Eng. Asp* **2021**, *615*, 126155.

[43] Qing, Y.;Shi, S.;Lv, C.; Zheng, Q. Microskeleton-nanofiller composite with mechanical super-robust superhydrophobicity against abrasion and impact. *Adv. Funct. Mater.* **2020**, *30*, 1910665.

[44] Hu, C.;Chen, W.;Li, T.;Ding, Y.;Yang, H.;Zhao, S.;Tsiwah, E. A.;Zhao, X.; Xie, Y. Constructing non-fluorinated porous superhydrophobic SiO_2-based films with robust mechanical properties. *Colloids Surf. A Physicochem. Eng. Asp.* **2018**, *551*, 65-73.

[45] Dai, Z.;Chen, G.;Ding, S.;Lin, J.;Li, S.;Xu, Y.; Zhou, B. Facile formation of hierarchical textures for flexible, translucent, and durable superhydrophobic film. *Adv. Funct. Mater.* **2021**, *31*, 2008574.

[46] Li, F.;Kong, W.;Bhushan, B.;Zhao, X.; Pan, Y. Ultraviolet-driven switchable superliquiphobic/superliquiphilic coating for separation of oil-water mixtures and emulsions and water purification. *J. Colloid Interface Sci.* **2019**, *557*, 395-407.

[47] Zhang, Z.;Yu, D.;Xu, X.;Yang, H.;Wyman, I.;Wang, J.; Wu, X. Versatile snail-inspired superamphiphobic coatings with repeatable adhesion and recyclability. *Chem. Eng. Sci.* **2021**, *230*, 116182.

[48] Chen, Y.;Liu, W.;Xu, C.;Liu, Y.;He, J.;Tian, D.;Long, L.;Yang, G.;Zhang, X.; Zhang, Y. Synthesis of a novel superamphiphobic coating with a hierarchical three-dimensional structure inspired by bird's nest. *Appl Clay Sci* **2021**, *204*, 106031.

[49] Krumpfer, J. W.;Bian, P.;Zheng, P.;Gao, L.; McCarthy, T. J. Contact angle hysteresis on superhydrophobic surfaces: an ionic liquid probe fluid offers mechanistic insight. *Langmuir* **2011**, *27*, 2166-2169.

[50] Li, S.;Page, K.;Sathasivam, S.;Heale, F.;He, G.;Lu, Y.;Lai, Y.;Chen, G.;Carmalt, C. J.; Parkin, I. P. Efficiently texturing hierarchical superhydrophobic fluoride-free translucent films by AACVD with excellent durability and self-cleaning ability. *J. Mater. Chem. A* **2018**, *6*, 17633-17641.

[51] Celik, N.;Torun, I.;Ruzi, M.;Esidir, A.; Onses, M. S. Fabrication of robust superhydrophobic surfaces by one-step spray coating: Evaporation driven self-assembly of wax and nanoparticles into hierarchical structures. *Chem. Eng. J.* **2020**, *396*, 125230.

[52] Bi, J.;Hao, Y.;Yang, L.;Zheng, Y.; Li, L. Impact of hydrophobicity on wetting characteristics of composite insulators. *IEEE Access* **2020**, *8*, 159316-159323.

[53] Xu, W.;Li, J.;Huang, Z.; Wang, F. Low water adhesion enhances the pollution flashover performance of superhydrophobic coating. In *IEEE Conference on Electrical Insulation and*

Dielectric Phenomena (CEIDP), 2020; pp 151-154.

[54] Xue, J.;Wang, H.;Chen, J.;Li, K.;Liu, B.;Song, B.;Deng, J.; Zhang, G. Effects of surface roughness on surface charge accumulation characteristics and surface flashover performance of alumina-filled epoxy resin spacers. *J. Mater. Chem. A* **2018**, *124*, 083302.